Predicting Power System Voltage Health Index with PMUs and Graph Convolutional Networks

Koji Yamashita, Jingtao Qin, and Nanpeng Yu
Electrical and Computer Engineering
University of California Riverside
Riverside, U.S.A.

Evangelos Farantatos and Lin Zhu
Transmission Operations and Planning R&D Group
Electric Power Research Institute
Knoxville, U.S.A.

***Abstract*—This paper develops a power system voltage health index prediction model using the graph convolutional network (GCN). Different power system operating conditions with varying loading levels and online generation are served as inputs to infer the system voltage health. Dynamic voltage responses captured by the time-domain simulation are used for four voltage indicators and their corresponding labels for training samples. The ordinal encoder is integrated after the output layer of the GCN model to introduce inductive bias in the learning process. The IEEE 14-bus standard model is adopted to evaluate the voltage health index prediction performance of the proposed GCN and baseline method. The prediction accuracy of the GCN is 15-27% higher than that of the baseline method. The partial observability from phasor measurement units was also hypothesized and it was revealed that GCN model prediction performance was preserved when measurement errors are accounted for in the range of -6% and +6%.**

***Index Terms*—Dynamic simulation, graph convolutional network, graph neural network, heath index, PMU, power system.**

I. Introduction

Rapid penetration of renewable energy resources represent a growing global concern for power system operations. Specifically, power grid operators must account for increasing contingency scenarios to evaluate the grid health following contingencies with ever-changing grid operating conditions. The key to improving the monitoring of transmission systems is the combination of advanced real-time grid sensors and data-driven grid health index prediction algorithms. Phasor measurement units (PMUs) are one of the most promising grid sensors and are widely deployed in the transmission grids around the world. These high-resolution sensors enable the development of data-driven algorithms to infer the health of the grid operating condition in real-time.

Numerous research studies leverage machine learning algorithms to analyze grid reliability by predicting system stress and health index [1]–[14]. Most of the existing data-driven approaches are designed to examine the rotor angle stability phenomenon. However, dynamic voltage health indices are less highlighted [1]. Various machine learning algorithms, such as tree-based methods, neural networks, least absolute shrinkage and selection operator (LASSO), support vector machine (SVM), have been extensively used to perform fast contingency analysis and evaluate grid heath index. A decision tree-based method was developed to perform online contingency analysis with the aim to extract the top eight critical contingencies based on the critical clearing time [2]. Although this approach evaluates both the transient stability and short-term voltage stability indices under various loading conditions, the grid structure is not explicitly considered. A convolutional neural network (CNN) is built to predict the angular stability-based health index, which categorizes each contingency as stable, critical stable or unstable using time-domain simulation results [3], [4]. Although the dynamic response is reflected in the CNN model via cascaded data windows, the only inputs this model considered are the rotor angles. Multi-step adaptive LASSO algorithm is applied to perform fast contingency screening and ranking for static security assessment [6]. Although the proposed algorithm is trained with all kinds of pre-contingency conditions (power flow, bus voltage, tap position, etc.) in the IEEE 118-bus and 300-bus system models, the dynamic response is missing. A data mining algorithm called core vector machine (i.e., a fast SVM) is adopted to solve the binary transient stability classification problem using massive amounts of PMU data [7]. Although cutting-edge preprocessing techniques are used to handle measurement noise and transients/spikes in PMU data, the algorithm assumes full coverage of PMUs at all power stations and substations. Reference [8]–[12] provides a comprehensive review of machine learning-based contingency analysis algorithms. Reference [8] concludes that the time-varying grid structure and system operating conditions have not been fully explored in data-driven system monitoring and dynamic studies.

To fill the aforementioned knowledge gap, this paper tries to evaluate the power system health index following contingencies with graph convolutional network, which captures both the changing power grid topology and system operating conditions. Furthermore, this paper focuses on evaluating power system voltage health index considering limited real-time observability through PMUs in the power network.

The main technical contributions of this paper are:

- The development of a graph convolutional network (GCN)-based voltage health index prediction algorithm, which significantly improves the prediction accuracy compared to

This project was sponsored by Electric Power Research Institute under agreement 10015026.

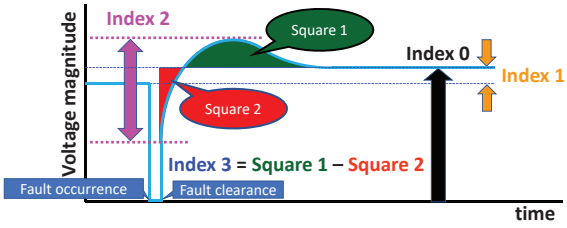

Fig. 1. Four voltage indices.

the state-of-the-art voltage heath index prediction method.

- The proposed GCN-based voltage health index prediction method is not only robust against erroneous measurement data but also can handle transmission systems with limited PMU observability.

The rest of the paper is organized as follows. Section II presents the proposed graph convolutional neural network for voltage health index prediction. Section III demonstrates the proposed algorithm in a case study using a standard IEEE testing system. Section IV concludes the paper.

II. Graph Convolutional Network Model for Voltage Health Index Prediction

This section first introduces four voltage health indices and the corresponding labels. Then the design of a GCN model to predict voltage health indices is presented. Finally, an ordinal encoder layer that injects the inductive bias is described.

A. Voltage Health Indices and the Corresponding Labels

Four voltage heath indices are designed for power system monitoring, as shown in Fig. 1. The first index (index 0) captures the post-event voltage level to confirm if this voltage level is within the permissible range at steady-state. The second index (index 1) quantifies the gap between steady-state voltage levels before and after the event. The third index (index 2) measures the difference between the maximum and minimum voltage levels after the fault is cleared. The final index (index 3) calculates the discrepancy in square-based voltage deviations above and below the post-fault voltage level. Detailed labels for each voltage health index are defined by separating the continuous voltage index values into 6 different categories, as shown in Table I. The class labels are being predicted on an index-by-index basis and will be used as outputs of the GCN model. Thus, the voltage health index prediction task is formulated as a classification problem.

B. GCN-based Voltage Health Index Prediction Model

There are two categories of inputs to the voltage health prediction model. The first category of inputs represent the pre-fault steady-state system information associated with the buses and branches. The second category of inputs indicates the contingency information which is encoded as the grid connectivity status of each branch. If a contingency affects a particular line segment or transformer, the grid connectivity status of the branch will change. Note that detailed input features for nodes and edges shown in Table II are assumed to be collected from PMUs.

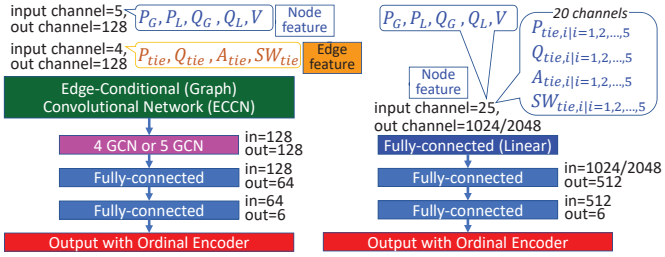

Fig. 2. GCN model (left) and MLP model (right).

The GCN [15] is selected as the deep learning model for the voltage health index prediction for a number of reasons. First, the GCN has been shown to be a very effective supervised learning algorithm on graph-structured data. Second, by treating the power network as the learning graph, the physical topology information can be directly utilized in the learning process of the GCN. Third, by leveraging the edge-conditional filter, the proposed GCN-based model enables embracing not only the bus but also the branch features to encode both local and global network information. Finally, the complexity of the GCN model scales linearly with the number of graph edges.

The overall architecture of the proposed GCN model and a baseline multilayer perceptron (MLP) model are shown in Fig. 2. The MLP is selected as the baseline model. Unlike the GCN, the MLP cannot directly handle edge features. Therefore, all five edge features in Table II are projected to node features, which increases the number of inputs from 5 to 25 (Fig. 2).

Inputs of the GCN model are first fed into the edge-conditioned convolution (ECC) layer, which updates each nodal i's feature vector from x_i to x'_i. This is done by activating the sum of the product of the weight matrix and the feature vector, and the aggregation of nodal and feature vectors via a parameterized neural network, as shown in (1).

$$\boldsymbol{x}'_i = \sigma\left(\boldsymbol{W}\boldsymbol{x}_i + \sum_{j\in\mathcal{N}(i)} \boldsymbol{x}_j \cdot h_\Theta(\boldsymbol{e}_{i,j})\right), \tag{1}$$

TABLE I
Labels Set for Each Voltage Health Index

Label	Index 0	Index 1	Index 2	Index 3
1	(1.07, ∞]	(0.01, ∞]	(0.40, ∞]	(1.25, ∞]
2	(1.05, 1.07]	(0.005, 0.010]	(0.3, 0.4]	(1.0, 1.25]
3	(1.03, 1.05]	(0.00, 0.005]	(0.20, 0.30]	(0.10, 1.00]
4	(1.00, 1.03]	(-0.03, 0.00]	(0.10, 0.20]	(0.05, 0.10]
5	(0.9, 1.0]	(-0.13, -0.03]	(0.0, 0.1]	(0.025, 0.050]
6	[-∞, 0.90]	[-∞, -0.13]	[-∞, 0.00]	[-∞, 0.025]

TABLE II
Inputs of GCN Model

	Bus features	Branch features
1	Active power output, P_G	Active power transfer, P_{tie}
2	Reactive power output, Q_G	Reactive power transfer, Q_{tie}
3	Active power load, P_L	Voltage angle difference bet. nodes, A_{tie}
4	Reactive power load, Q_L	Grid connectivity status, SW_{tie}*
5	Voltage magnitude	

* line disconnections: status changes from 1 to 0.5 (see Section III-A-1)), transformer tripping: status changes from 1 to 0.

Algorithm 1 Classification with Ordinal Encoder

for every epoch **do**

K logits L_i are derived at the last layer

$s_i = sigmoid(L_i), \forall 1 \leq i \leq K$

$L'_i = \sum_{j \leq i} \log(s_j) + \sum_{i<j} \log(1 - s_j), \forall 1 \leq i \leq K$

$p'_i = \text{softmax}(L'_i), \forall 1 \leq i \leq K$

end for

where $\boldsymbol{W}$ denotes weight matrix, h_Θ denotes a neural network (e.g., a multilayer perceptron), $\boldsymbol{x}_i$ denotes the feature vector of the i-th node, and $\boldsymbol{e}_{i,j}$ denotes the feature vector for the edge from the source node, i, to the target node, j. σ denotes the activation function, which is selected to be Relu in our proposed model.

The output of the ECC layer is then fed into a number of graph convolutional layers (highlighted in pink in Fig. 2) and fully-connected layers. The nodal representations $\boldsymbol{x}_i$ are updated in each of the graph convolutional layers following (2).

$$\boldsymbol{x}'_i = \sigma\left(\widetilde{\boldsymbol{W}}^{\boldsymbol{T}} \sum_{j \in \nu} \frac{\hat{A}_{j,i}}{\sqrt{\hat{d}_j \hat{d}_i}} \boldsymbol{x}_j\right)$$

$$\hat{d}_i = 1 + \sum_{j \in \mathcal{N}(i)} \hat{A}_{j,i}, \quad \hat{d}_j = 1 + \sum_{i \in \mathcal{N}(j)} \hat{A}_{i,j}, \tag{2}$$

where ν denotes the set of all adjacent nodes of the graph. $\hat{A}_{i,j}$ denotes an ij-the element of $\hat{A} = A + 1$, where A is the adjacency matrix. $A_{i,j}$ equals to 1 if node i is connected to node j and 0 otherwise.

C. Ordinal Encoder

The labels in each voltage health index can be described as an ordinal variable. For example, the difference between system voltage health for label 4 and 5 is much smaller than that of level 4 and 1. Thus, ordinal encoding can be adopted to introduce inductive bias that represents the natural ordering between the labels in each voltage index. To implement the ordinal encoder, we take the output logits L_i from the last fully-connected layer and run it through Algorithm 1 to derive the probability that the voltage health index belongs to each of the $K = 6$ labels. Since the grid voltage health index prediction task is formulated as a classification problem, the cross-entropy loss function is selected for gradient calculations.

III. Numerical Study

In this section, the setup of numerical study is first described in detail. The voltage health index prediction results of the proposed and baseline models are then presented.

A. Case Study Setup

The setup of the testing transmission system, contingency scenarios, operating conditions, dynamic models, and the PMU coverage are explained below.

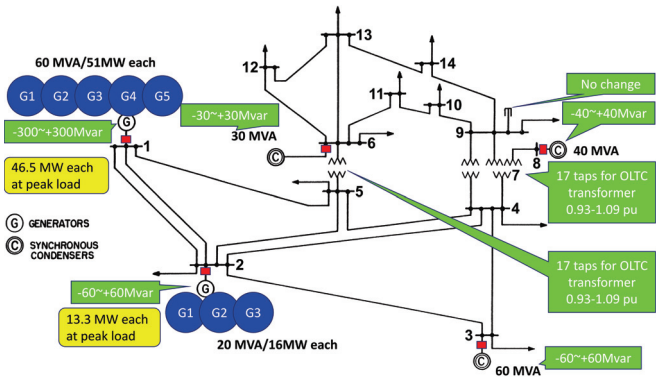

Fig. 3. IEEE 14-bus test system.

1) Test System and Contingency Scenarios: The IEEE 14-bus system [16], shown in Fig. 3, is adopted as the testing environment in this study. In this initial work, the primary focus is on examining the N-1 contingencies, which can be categorized into two groups: single line outage out of double circuit lines following 3-phase ground faults and transformer outage with balanced inter-turn short-circuit faults. Note that the fault duration is set to 50 ms. The generator outage is out of the scope of this study because it is likely to cause frequency stability problems. As shown in Fig. 3, a double circuit line is explicitly displayed only between buses 1 and 2. All lines in the testing system are assumed to be parallel double-circuit lines except the transmission line between buses 1 and 2. In this case, the number of lines that are subject to the contingency halves after the fault clearance. All step-down transformers are disconnected after the fault is cleared. In total, there are 19 outages (15 line outages and 4 transformer outages) on the contingency for this test system.

2) Scenarios of System Operating Conditions: Based on the given peak load profile in [16], a three-step process is used to generate a wide range of system operating conditions: a) varying loading conditions; b) various power station-level dispatch cases; c) different unit-level dispatch scenarios.

a) Loading conditions: Various loading conditions are created by scaling the total system demand between 40% and 100% of the peak demand with an increment of 5%.

b) Power plant dispatch: It is assumed that there are 5 and 3 generator units connected to Buses 1 and 2. It is further assumed that the nameplate capacity of each generator at Buses 1 and 2 are 60 MVA (51 MW) and 20 MVA (16 MW), respectively. To create 18 different power plant dispatch scenarios for each system loading condition, the output of each unit at Bus 1 is gradually increased from 13.1 MW to 46.5 MW while the output of each unit at Bus 2 is decreased from 13.3 MW to 2 MW.

c) Unit-level dispatch scenarios: There are two unit level dispatch scenarios: even unit dispatch and uneven unit dispatches. The even unit dispatch scenario means that the active power outputs of all units at the same Bus are kept the same. In contrast, under the uneven unit dispatch scenario, one of the generators at Bus 1's output level is adjusted higher or lower while the remaining generators have the same active

TABLE III
VOLTAGE HEALTH INDICES PREDICTION PERFORMANCE USING GCN (LEFT) AND MLP (RIGHT)

Volt. health index	Validation loss ($\times 10^{-5}$)	Testing accuracy	# of neurons in hidden layers	# of hidden layers	Learning rate of Adam ($\times 10^{-3}$)
0	0.586/3.510	**0.966**/0.811	128/2048	5/4	1.4/2.0
1	1.120/6.196	**0.930**/0.689	128/1024	5/1	1.8/1.6
2	2.116/7.655	**0.844**/0.594	128/1024	6/1	2.0/2.0
3	1.830/7.708	**0.899**/0.620	128/1024	6/1	2.0/2.0

power outputs.

It is noted that the reactive power balance and voltage magnitude are within the constraints for all simulation scenarios by adjusting the on-load tap changers and reactive power output from synchronous generators/condensers. Also note that during the peak load condition, only one power plant and dispatch condition exists under the even dispatch scenario.

In sum, the total number of simulation scenarios is 8227, which is further split into 6587 (80%), 820 (10%), and 820 (10%) cases for training, validation, and testing, respectively.

3) Dynamic Models: The dynamic model is built for a round rotor generator with one damper winding circuit for each of the D-axis and Q-axis (with no saturation). A DC exciter (i.e., automatic voltage regulator) model without a power system stabilizer is included. A simplified governor model and an exponential load model with indices of 1 and 2 are adopted for active and reactive power, respectively. The parameters set for generator controllers in this study are all standardized built-in values of commercially available software [17].

4) PMU Coverage: Although PMUs are being widely deployed in the transmission grids, they may not be installed at every substation. Thus, it is crucial to examine the performance of the proposed voltage health index prediction model when a subset of substations do not have PMUs. Two approaches are employed to deal with the partial PMU coverage in the power grid. The first one is to leverage pseudo measurements from the state estimator outputs that are typically obtained every few seconds or minutes. The second one is to replace the data for non-existing PMUs with zero or peak values.

B. Voltage Health Index Prediction Results

1) GCN and MLP Model Performance: The validation losses and testing accuracies obtained from the GCN and the MLP models with edge features are reported in Table III. Regardless of the voltage health index, the GCN model always achieves a lower validation loss and much higher testing accuracy than the MLP model. By directly encoding the system topology information in a neural network, the proposed GCN-based model is able to significantly outperform the baseline MLP model. Note that the hyperparameters, such as the number of hidden layers, number of neurons, and learning rate, are selected using the validation dataset.

2) GCN-based Voltage Health Index Prediction with Partial PMU Coverage: Three cases with different PMU coverage in the power system are analyzed, as shown in Table IV. Case All-Buses represents the scenario where PMUs are installed

TABLE IV
CASE STUDIES WITH DIFFERENT PMU COVERAGE IN THE SYSTEM

Case	Missing PMU	Transmission	Sub-transmission
Bus-1x	Buses 10-14	full observability	partial observability
Bus-3	Bus 3 only	partial observability	full observability
All-buses	N/A	full observability	full observability

in every bus of the network. In Case Bus-1x, none of the substations in the sub-transmission system have PMUs. In Case Bus-3, one substation (Bus 3) in the transmission grid does not have PMUs. Below we show the performance of the proposed GCN with two different approaches to deal with the cases of partial observability.

a) Pseudo Measurements from the State Estimator: The necessary input data to the GCN model at the bus without PMU can be replaced with pseudo measurements from the state estimator. Typically, the state estimator results are refreshed every 0.5-5 minutes instead of every 1/30 seconds that is a typical PMU measurement reporting rate. Thus, the pseudo measurements from the state estimator can represent PMU measurements with errors that are comprised of measurement noise, state estimation error, and discrepancies between true values and delayed values caused by the time to collect data and transmit data. In the experiment, a Gaussian noise is added with standard deviation between 0.01 and 0.5 to the dynamic simulation results to emulate with the aforementioned errors in the pseudo measurements. Note that the standard deviation of 0.01 corresponds to ±3% measurement error. The testing losses and accuracy of voltage health index prediction are analyzed with different level of measurement noise.

The testing losses in Case Buses 1x and Case Bus-3 are shown in Fig. 4. It can be seen from these figures that the testing losses both increase as the standard deviation of the measurement noise becomes larger. The increase in testing loss is more dramatic when the transmission system (Bus 3) rather than sub-transmission system (Buses 10-14) lacks PMU coverage. Finally, when the standard deviation of the measurement noise is smaller than or equal to 0.1, the increase in testing loss is minimal.

The testing accuracies of the proposed GCN model without complete PMU coverage is shown in Fig. 5. As expected, the testing accuracy drops as the standard deviation of the measurement noise increases. Similarly, the drop in accuracy

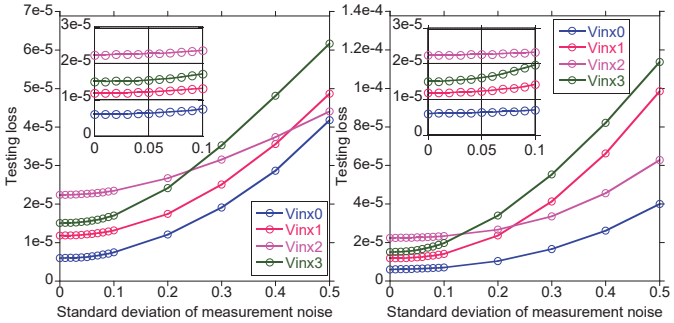

Fig. 4. Testing loss when no PMUs are available at Buses 10-14 (left) or Bus 3 (right).

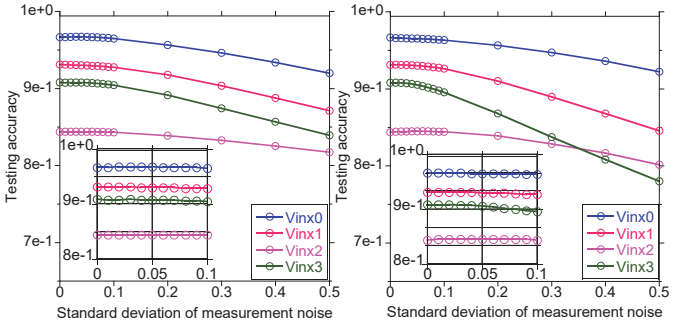

Fig. 5. Testing accuracy when no PMUs are available at Buses 10-14 (left) or Bus 3 (right).

is more significant when the transmission system rather than sub-transmission system loses the PMU measurements.

b) Zero/Peak Value Imputation for Substation(s) with no PMUs: Figures 6 and 7 show the testing losses and accuracies in Case Bus-1x and Case Bus-3. Both zero and peak value imputation strategies yield higher testing loss and lower testing accuracy than that of the pseudo measurement approach to deal with insufficient PMU coverage. When a large number of sub-transmission system buses (Buses 10-14) do not have PMU measurements, the peak value imputation strategy outperforms zero imputation strategy in predicting voltage health index. However, when only one major transmission system bus (94.2 MW of load) does not have PMU measurements, then the zero imputation strategy outmatches the peak imputation strategy.

IV. Conclusion

This work developed a graph convolutional network (GCN)-based voltage health index prediction algorithm to monitor a transmission system in real time operations. By inserting system topology information in the neural network and introducing ordinal encoding, the proposed GCN-based algorithm achieved significant performance improvement in testing accuracy (15-27%) over the baseline algorithm. The proposed GCN-based voltage health index prediction algorithm can also monitor transmission grids with limited PMU observability. Pseudo measurements obtained from the output of the state estimator are reasonable replacements for the PMU measurements for the purpose of estimating voltage health indices. Even naive zero or peak imputation strategy could provide fair results under certain circumstances. In the future, we plan to further extend this research work by considering N-k contingencies in larger system models and other types of system health indices (e.g., frequency stability index and angular stability index) in a holistic manner. In addition, extra physical priors could be embedded in the neural network as inductive bias to improve the scalability and generalization capability of the proposed algorithm on larger testing systems with unforeseen system configurations.

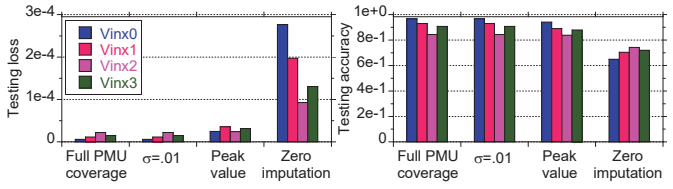

Fig. 6. Testing loss and accuracy when Buses 10-14 have no PMU.

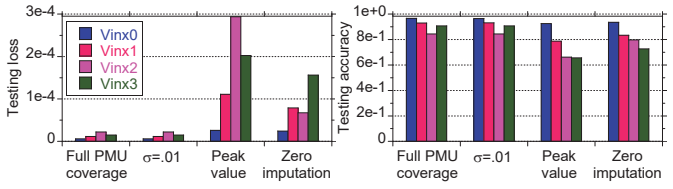

Fig. 7. Testing loss and accuracy when Bus 3 has no PMU.

References

[1] H. Hagmar, lang Tong, R. Eriksson, and L. A. Tuan, "Voltage instability prediction using a deep recurrent neural network," *IEEE Trans. Power Syst.*, vol. 36, no. 1, pp. 17–27, Jan. 2021.

[2] C. Liu, K. Sun, Z. H. Rather, Z. Chen, C. L. Bak, P. Thøgersen, and P. Lund, "A systematic approach for dynamic security assessment and the corresponding preventive control scheme based on decision trees," *IEEE Trans. Power Syst.*, vol. 29, no. 2, pp. 717–730, Mar. 2014.

[3] R. Yan, G. Geng, Q. Jiang, and Y. Li, "Fast transient stability batch assessment using cascaded convolutional neural networks," *IEEE Trans. Power Syst.*, vol. 34, no. 4, pp. 2802–2813, Jul. 2019.

[4] Y. Zhao, S. You, M. Mandich, L. Zhu, C. Zhang, H. Li, Y. Su, Y. Liu, H. Jiang, H. Yuan, Y. Zhang, and J. Tan, "A fast and accurate transient stability assessment method based on deep learning: Wecc case study," in *Proc. of IEEE PES Innov. Smart Grid Technol. US*, Apr. 2022.

[5] B. Donnot, I. Guyon, M. Schonauer, P. Panciatici, and A. Marot, "Power grid contingency analysis with machine learning: A brief survey and prospects," in *Proc. of Int. Jt. Conf. Neural Netw. (IJCNN)*, Jul. 2018.

[6] Y. Li, Y. Li, and Y. Sun, "Online static security assessment of power systems based on lasso algorithm," *Applied Sciences*, Aug. 2018.

[7] B. Wang, B. Fang, Y. Wang, H. Liu, and Y. Liu, "Power system transient stability assessment based on big data and the core vector machine," *IEEE Trans. Smart Grid*, vol. 7, no. 5, pp. 2561–2570, Sep. 2016.

[8] S. Yang, B. Vaagensmith, and D. Patra, "Power grid contingency analysis with machine learning: A brief survey and prospects," in *Proc. of 2018 Int. Jt. Conf. Neural Netw. (IJCNN)*, Oct. 2020.

[9] L. Duchesne, E. Karangelos, and L. Wehenkel, "Recent developments in machine learning for energy systems reliability management," *Proc. IEEE*, vol. 108, no. 9, Sep. 2020.

[10] J. L. Cremer and G. Srbac, "A machine-learning based probabilistic perspective on dynamic security assessment," *Int. J. Electr. Power Energy Syst*, vol. 128, p. 106571, Jan. 2021.

[11] Z. Shi, W. Yao, Z. Li, L. Zeng, Y. Zhao, R. Zhang, Y. Tang, and J. Wen, "Artificial intelligence techniques for stability analysis and control in smart grids: Methodologies, applications, challenges and future directions," *Applied Energy*, vol. 278, p. 115733, Sep. 2020.

[12] M. Nazari-Heris, S. Asadi, B. Mohammadi-Ivatloo, M. Abdar, H. Jebelli, and M. Sadat-Mohammadi, *Application of machine learning and deep learning methods to power system problems*, 1st ed. Switzerland: Springer, 2022.

[13] J. J. Q. Yu, D. J. Hill, A. Y. S. Lam, J. Gu, and V. O. K. Li, "Intelligent time-adaptive transient stability assessment system," *IEEE Trans. Power Syst.*, vol. 33, no. 1, pp. 1049–1058, Jan. 2018.

[14] L. Zhu, D. J. Hill, and C. Lu, "Hierarchical deep learning machine for power system online transient stability prediction," *IEEE Trans. Power Syst.*, vol. 35, no. 3, pp. 2399–2411, May 2020.

[15] T. N. Kipf and M. Welling, "Semi-supervised classification with graph convolutional networks," in *Proc. of 5th Int. Conf. on Learning Representations (ICLR)*, Apr. 2017.

[16] Power Systems Test Case Archive. (Aug., 1993) 14 bus power flow test case. University of Washington. [Online]. Available: https://www2.ee.washington.edu/research/pstca/pf14/pg_tca14bus.htm

[17] K. Yamashita, C.-W. Ten, and L. Wang, "Dynamical analysis of cyber-related contingencies initiated from substations," in *Security of Cyber-Physical Systems*, H. Karimipour, P. Srikantha, H. Farag, and J. Wei-Kocsis, Eds. Springer, Cham, 2020, pp. 223–246. [Online]. Available: https://doi.org/10.1007/978-3-030-45541-5_12.